

Multiojective Optimization of a Hollow Plunger Type Solenoid for High Speed On/Off Valve

Shuai Wu¹, Member, IEEE, Xiangyu Zhao, Chunfang Li, Zongxia Jiao, Senior Member, IEEE, and Fengyu Qu

Abstract—This paper presents the modeling, optimization, and validation of a hollow plunger type solenoid for high speed On/Off valve. In the preliminary design, an accurate equivalent magnetic circuit model of the proposed solenoid is carried out, and the magnetic circuit is arranged in Kirchhoffs voltage law matrix form for the convenience of computer calculation. An iterative method is applied to obtain accurate permeability of the nonlinear magnetic material. To optimize the design parameters, a multiobjective optimization process is developed, and the multiobjective particle swarm optimization method is used to obtain the Pareto front of the desired objectives. An approved solution in Pareto front is selected by analytic hierarchy process and validated by the finite element analysis (FEA) method. A prototype based on the final optimized design is manufactured and tested. The experiment results verified the validation proposed design and optimization process.

Index Terms—Equivalent magnetic circuit (EMC), finite-element analysis (FEA), high speed on/off valve (HSV), multiobjective optimization (MOO), solenoid.

I. INTRODUCTION

THE conventional electro-hydraulic servo system usually uses servo valve as the control component. The servo valve has advantages of high precision, low dead zone, and small hysteresis, which bring high control performance, but the disadvantages of servo valve include high cost, low efficiency, and low reliability due to being sensitive to oil containments. Therefore, digital hydraulic system that uses a combination of high speed On/Off valves (HSV) to replace the servo valve is a developing trend. The electro-hydraulic system controlled by HSV has several benefits over that with servo and proportional valves: They are inexpensive, reliable, insensitive for contamination, and possibly zero leakage [1]. HSV can be used in hydraulic pulse width modulation control, and the flow rate can

be continuously controlled through adjusting pulse frequency and pulse width. Digital hydraulic system can improve the efficiency significantly, which makes HSV become an research hotspot hydraulic field recently [2]–[5]. However, the HSV still needs to improve to meet the requirements of digital hydraulic servo system, such as quicker response, and smaller size.

The opening and closing time are the most important indicators of HSV. In order to shorten opening time, some smart materials, such as giant magnetostrictive material and piezoelectric crystals with advantage of quick response, are used in the HSV [6]–[9], but these materials still have some disadvantages, which limited its widely application, such as high cost and too small stroke. On the contrary, electromagnetic actuator driving HSV is more feasible but the response is relatively slow. Solenoid is a common used electromagnetic actuator in hydraulic valve due to its simple structure and low cost. It has been made a great progress in the past decades and various types of solenoid have been investigated in [10]–[12]. Some solenoid driving on/off valve can now meet the 5 ms opening and closing time requirement, but it still needs to be improved for new applications, such as digital hydraulic system.

This study aims at developing a new solenoid driving HSV and optimizing the performances of response time, size, and thermal performance. Since these objectives are usually conflicted with each other, therefore multiobjective optimization (MOO) method in which all objectives are being considered simultaneously is required. For MOO problems, a common way is using a set of weighting coefficients to trade off different objectives [13], [14], but more advanced methods often involve artificial intelligence methods to obtain the Pareto front of the objectives under design constraints [15]–[18].

The magnetic field calculation is the foundation for optimization of solenoid that can be obtained by methods of finite-element analysis (FEA), analytical model calculation, etc. The FEA method can directly calculate the flux pattern with high accuracy, and it is usually applied in the detailed design phase for specification purposes, such as motor geometry parameters optimization [19]. However, the entire process of FEA is usually computationally expensive [20], [21]. Moreover, changing the design parameters in FEA, especially the structure parameters in the preliminary design phase, often requires the model to be reconstructed. On the other hand, an analytical approach can allow the researcher to change parameters conveniently with respect to the given requirements and constraints [22], [23]. The equivalent magnetic circuit (EMC) method that is a typical

Manuscript received January 28, 2017; revised April 17, 2017 and July 4, 2017; accepted August 7, 2017. Date of publication September 29, 2017; date of current version January 5, 2018. This work was supported in part by the National Key Basic Research and Development Program under Grant 2014CB046401, in part by the National Natural Science Foundation of China under Grant 51235002, and in part by the Industrial Foundation Enhancement Project Grant TC150B5C0-29-04. (Corresponding author: Wu Shuai.)

The authors are with the School of Automation Science and Electrical Engineering, Beihang University, Beijing 100191, China (e-mail: wushuai.vip@gmail.com; zhaoxiangyu@buaa.edu.cn; lichunfang001@buaa.edu.cn; zxjiao@buaa.edu.cn; quyufeng@buaa.edu.cn).

Color versions of one or more of the figures in this paper are available online at <http://ieeexplore.ieee.org>.

Digital Object Identifier 10.1109/TIE.2017.2756578

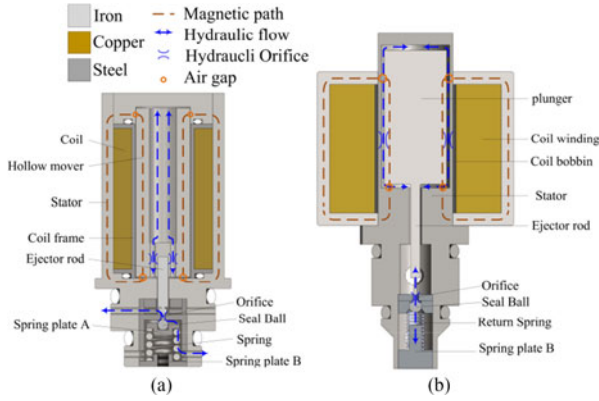


Fig. 1. Comparison of structure of proposed HSV and conventional HSV. (a) Proposed HSV. (b) Conventional HSV.

analytical approach often serves as the first step in the analysis and design of electric machines [24]–[27]. The EMC model is often incorporated with other methods, such as FEA for further confirmation of the calculation results [28]–[30].

The purpose of this study is to develop a HSV to meet the requirements of digital hydraulic system. The main challenges include quick response (opening and closing time should less than 3 ms), small size and low working temperature. In order to achieve these goals, a new structure solenoid is proposed. The new design uses a hollow plunger type solenoid to replace conventional solid one, which can reduce the magnetic resistance and enhance the output force. For the proposed solenoid, there are several parameters should be determined, which influence the performance significantly and usually conflict with each other. In order to optimize these parameters, a high accuracy EMC model, which considered the nonlinearity of iron material, and arranged in the Kirchhoff voltage law (KVL) matrix format for computational efficiency, is studied. The kinetic dynamic model and thermodynamic model that can get the relation between design parameter and performance are also discussed. Based on the these models, a MOO design process is carried out which obtaining the Pareto front of desired objectives first, and then, an best solution in the Pareto front is selected by multi-objective decision-making (MOD) method. Finally, a prototype based on the optimized parameters is manufactured and tested. The experimental results verify the effectiveness and validity of the proposed design and optimization approach.

II. STRUCTURE OF PROPOSED SOLENOID

The structure of the proposed HSV is shown in Fig. 1(a) and a typical conventional structure is shown in Fig. 1(b) for comparison. It is a two position on/off valve. The returning spring pushes the ball to seal orifice when coil has no current. The plunger generates force and move down when the coil is powered and push away the ball to open the orifice. The main innovation of the proposed HSV is the solenoid using a hollowed type plunger to replace the solid plunger. The hole in the middle of the plunger is used to connect the chambers in two ends which allows the oil to pass through when the plunger is moving. The conventional solenoid usually let the oil through the peripheral

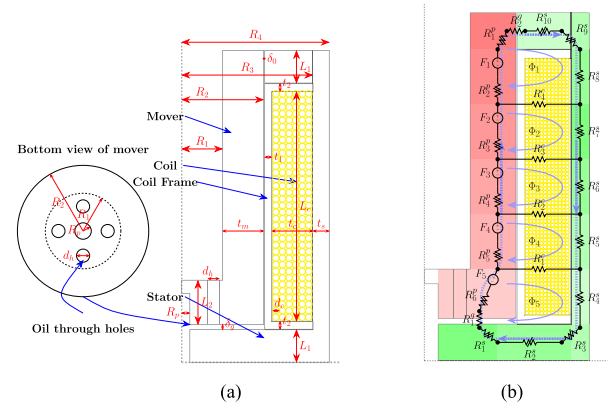


Fig. 2. Geometry diagram and equivalent magnetic circuit model of proposed HSV. (a) Geometry definitions of HSV. (b) Geometry definitions of HSV.

clearance, but it introduces unwanted air gap which weakens the magnetic force. The proposed design can minimize this unwanted peripheral air gap and enhance the magnetic force. Meanwhile, the hollow design also reduces the mass of mover which can short the response time further. The simulation results in present study also indicates that the hollow holes has little influence on the magnetic force.

III. ANALYTICAL MODELING BY EMC

A. Geometry Definitions and EMC Modeling

The simplified geometry diagram and parameter definitions of proposed HSV is shown in Fig. 2(a). The EMC model of proposed HSV is shown in Fig. 2(b). The symbol definitions in Fig. 2(b) include magneto-motive force (MMF) F_i , equivalent magnetic reluctance R_i , and magnetic flux ϕ_i .

F_i MMF in loop i .

ϕ_i magnetic flux in loop i .

R_i^* equivalent magnetic reluctance in loop i of different parts by symbol * to distinguish them. Symbol p means plunger, g means air gap, s means shell, and c means coil.

In the EMC method, the accuracy of the results depends on the correction of the built model. Generally, magnetic flux prefers to pass through the material with high magnetic permeability, which is similar to the current in the conductor. Usually, only the main magnetic loop is taken into account for simplicity, but in fact, part of the magnetic flux overflows from the main circuit and leaks through the winding. Therefore, a more accurate model with considering the leakage flux is developed in the present study. The magnetic circuit is like a electrical network that is made up of several voltage sources and resistances. The circuit like this can be solved by KVL matrix method.

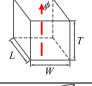
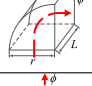
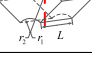
The MMF sources of winding current are given by

$$F_i = N_i I \quad n = 1, 2, \dots, 5 \quad (1)$$

where N_i is the winding turns in the loop i . It can be calculated by

$$N_i = \text{floor} \left(\frac{L_i}{C_d} \right) \times \text{floor} \left(\frac{R_3 - R_2 - t_1}{C_d} \right). \quad (2)$$

TABLE I
CALCULATION OF RELUCTANCE OF EMC MODEL

Reluctances	Shape	Equation	Schematic
$R_{2\sim6}^p, R_{4\sim8}^s, R_1^g$	Cuboid	$R = \frac{T}{\mu WL}$	
$R_1^p, R_1^s, R_3^s, R_9^s$	Axial Quarter Cylinder	$R = \frac{\pi}{4\mu L}$	
$R_2^s, R_{1\sim4}^c, R_{10}^s, R_2^g$	Radial Quarter Cylinder	$R = \frac{\ln(\frac{r_2}{r_1})}{2\mu\pi L}$	

Basic expression of reluctances is given by

$$R = l/\mu s \quad (3)$$

where l is the length of flux path, μ is the permeability of the materials, and s is the section area of flux path. The reluctances can be classified into three types by shapes, which are listed in **Table I** [31].

The detail equations of each reluctances of plunger are listed below. The symbols used in the following equations are $T = (L_c + 2t_2 - L_3 - \delta_g)/4$, $s_p = \pi(R_2^2 - R_1^2)$, $s_s = \pi(R_4^2 - R_3^2)$, $s_g = \pi(R_2^2 - R_p^2 - d_h^2)$. The reluctances of each part can be calculated by the following equations:

$$R_1^p = \frac{1}{4\mu_1^p(R_1 + R_2)} \quad (4)$$

$$R_i^p = \frac{T}{\mu_i^p s_p} \quad i = 2, 3, \dots, 5 \quad (5)$$

$$R_6^p = \frac{L_3}{\mu_6^p s_g} \quad (6)$$

The reluctances of shell can be presented in the following equations:

$$R_1^s = \frac{1}{4\mu_1^s(R_p + R_2)} \quad (7)$$

$$R_2^s = \frac{\ln \frac{2R_3}{R_1 + R_2}}{2\mu_2^s \pi L_2} \quad (8)$$

$$R_3^s = \frac{1}{8\mu_3^s R_3} \quad (9)$$

$$R_4^s = \frac{L_3 + \delta_g}{\mu_4^s s_s} \quad (10)$$

$$R_i^s = \frac{T}{\mu_i^s s_s} \quad i = 5, 6, \dots, 8 \quad (11)$$

$$R_9^s = \frac{1}{8\mu_9^s R_3} \quad (12)$$

$$R_{10}^s = \frac{\ln \frac{R_3}{R_2}}{2\mu_{10}^s \pi L_1} \quad (13)$$

The reluctance of coil R_2^g is radial quarter cylinder and the reluctance of the air gap R_1^g is cuboid, which can be calculated

by the following equations:

$$R_1^c = \frac{\ln \frac{R_3}{R_2}}{2\mu_1^c \pi (0.5T + L_3 + \delta_2)} \quad (14)$$

$$R_i^c = \frac{\ln \frac{R_3}{R_2}}{2\mu_i^c \pi T} \quad i = 2, 3 \quad (15)$$

$$R_4^c = \frac{\ln \frac{R_3}{R_2}}{2\mu_4^c \pi 1.5T} \quad (16)$$

$$R_2^g = \frac{\ln \frac{R_2 + \delta_0}{R_2}}{2\mu_2^g \pi L_1} \quad (17)$$

$$R_1^g = \frac{\delta_g}{\mu_1^g s_p} \quad (18)$$

By the calculation of reluctances and MMFs, the EMC model can be expressed in matrix form presented below and can be solved by the KVL method:

$$\mathbf{R}\Phi = \mathbf{F} \quad (19)$$

The reluctance matrix \mathbf{R} is presented as

$$\mathbf{R}_{5 \times 5} = \begin{bmatrix} R_{1,1} & -R_4^c & 0 & \dots & 0 \\ -R_4^c & R_{2,2} & -R_3^c & \dots & 0 \\ \vdots & & & \ddots & 0 \\ 0 & \dots & -R_2^c & R_{4,4} & -R_1^c \\ 0 & \dots & 0 & -R_1^c & R_{5,5} \end{bmatrix} \quad (20)$$

The vector of magnetic flux Φ is presented as

$$\Phi_{5 \times 1} = [\Phi_1, \Phi_2, \dots, \Phi_5]^T \quad (21)$$

The vector of MMF source \mathbf{F} is presented as

$$\mathbf{F}_{5 \times 1} = [F_1, F_2, \dots, F_5]^T \quad (22)$$

where the reluctances $R_{i,j}$ in matrix \mathbf{R} can be calculated by

$$R_{1,1} = R_1^p + R_2^p + R_8^s + R_9^s + R_{10}^s + R_2^g + R_4^c$$

$$R_{2,2} = R_3^p + R_7^s + R_3^c + R_4^c$$

$$R_{2,2} = R_4^p + R_6^s + R_2^c + R_3^c$$

$$R_{4,4} = R_5^p + R_5^s + R_1^c + R_2^c$$

$$R_{5,5} = R_6^p + R_1^s + R_2^s + R_3^s + R_4^s + R_1^g + R_1^c$$

The vector of flux (Φ) can be obtained by the following equation:

$$\Phi = \mathbf{F}\mathbf{R}^{-1} \quad (23)$$

Then the flux density at each segment (B_i) can be obtained by

$$B_i = \Phi_i / S_i \quad (24)$$

B. Nonlinear Material Consideration

The shell and plunger should be made by ferromagnetic material with low magnetic retentivity, low hysteresis loss, and high saturation magnetic flux density. Therefore, soft iron (material

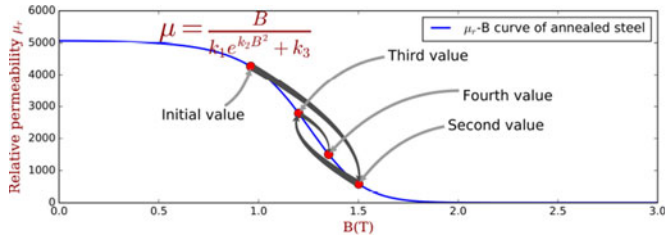


Fig. 3. Curve of relative permeability versus flux density of soft iron.

type DT4) is chosen in the present study. Its permeability μ varies with the flux density resulting the B is not a linear proportion to H . So, the nonlinear material characteristic should be taken into account to obtain high accuracy simulation result. The relationship between permeability and magnetic flux density of iron is modeled by the following equation [28]:

$$\mu = B / (k_1 e^{k_2 B^2} + k_3) \quad (25)$$

where k_1 , k_2 , and k_3 are constants for $B-H$ curve of material. Fig. 3 shows the curve of relative permeability versus flux density of soft iron. To avoid flux saturation, the maximum flux density of the stator and plunger should not exceed the knee point of the $B-H$ curve.

An iterative method to update permeabilities is applied in the calculation process. The permeabilities of each segment will be initiated with a reasonable value and these values are used to calculate the flux density in the first loop. Then, update the permeabilities according to the calculated flux density by 25. After that, return to the step of calculation of flux densities with the new permeabilities. This loop is iterated until the permeabilities are converged. This process is shown in Fig. 3

$$\mu_{n+1} = B_n / (k_1 e^{k_2 B_n^2} + k_3). \quad (26)$$

A small final error ϵ is set to stop the iteration

$$|B_n - B_{n-1}| < \epsilon. \quad (27)$$

As Fig. 3 shows, the derivative of $B-H$ curve is monotonically decreasing, and therefore, this process will eventually converge to a definite point.

C. Validate EMC Model by FEA Method

Before the EMC model is applied for parameter optimization, it should be validated by a more accurate simulation method, such as FEA method. A typical design with parameters $R_4 = 9$ mm, $R_3 = 7.5$ mm, $R_2 = 4$ mm, $R_1 = 2$ mm, $R_p = 0.75$ mm, $L_1 = 3$, $L_2 = 3$ mm, $L_c = 20$ mm, $t_1 = 0.6$ mm, $t_2 = 0.5$ mm, and $\delta_0 = 0.05$ mm is simulated with FEA and EMC method, respectively and the simulation results are compared. The flux density distribution by FEA and the curve of force verse displacement are shown in Fig. 4. The curves of force verse displacement by the FEA and EMC method indicate that the accuracy of the proposed EMC model is entirely acceptable for preliminary design phase. The flux density distribution indicates that the fluxes are concentrated in the plunger close to the outer surface, that means the hollow design doesn't have that much impact on the flux density.

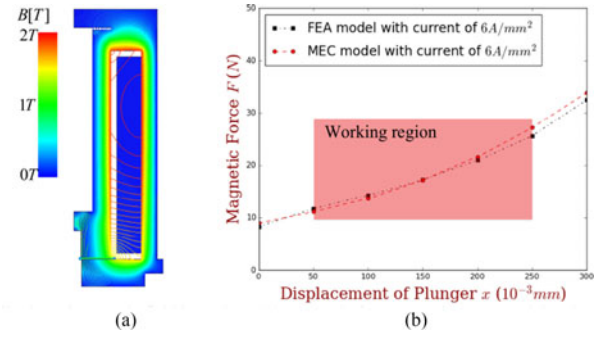


Fig. 4. Validation the EMC model with FEA approach. (a) Distribution of magnetic field intensity and magnetic field lines. (b) Magnetic force curve in MEC model and FEA model.

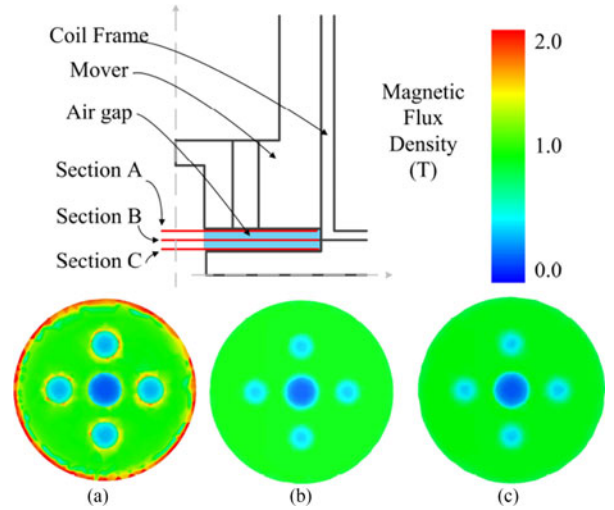


Fig. 5. Magnetic flux density distribute on different sections in air gap via 3-D FEM simulation. (a) Section A. (b) Section B. (c) Section C.

As Fig. 2(a) shows that the mover has holes to pass through the hydraulic flow. The holes will influence the electromagnetic force since they will influence the air gap flux density. This effect is validated by 3-D FEA. The flux density distribution on different sections in the air gap is shown in Fig. 5. The results indicate that the flux density in the hole is smaller than the other region. But, the distribution tends to be even when the section gets close to the stator. The output force of solenoid F_m can be expressed by the following equation:

$$F_m = \frac{s_g B_g^2}{2\mu_0} \quad (28)$$

where s_g is effective section area of air-gap, and B_g is magnetic flux density in air gap. In the present study, a conservative calculation method is applied where $s_g = \pi(R_2^2 - R_p^2) - \pi d_h^2$ is used as effective area.

IV. MULTIOBJECTIVES OPTIMIZATION

A. Optimization Parameters

In the present study, the designed stroke of plunger is $x_s = 0.2$ mm. The design parameters that should be decided

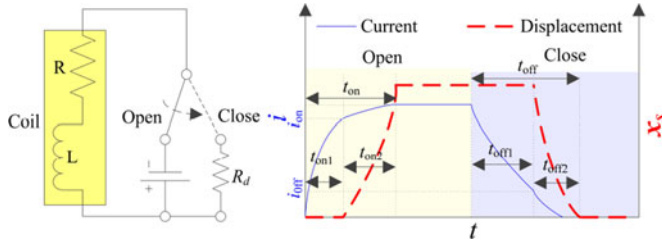


Fig. 6. Schematic diagram of opening and closing processes.

of the proposed solenoid are shown in Fig. 2(a). The predefined parameters include outer diameter $R_4 = 9$ mm, diameter $R_p = 0.75$ mm, length $L_2 = 5$ mm, thickness of $t_1 = 0.5$ mm and $t_2 = 0.5$ mm, clearance $\delta_0 = 0.05$ mm, initial air gap $\delta_g = 0.3$ mm, and diameter of oil through holes $d_h = 1$ mm. There are still six parameters that need to be optimized, which include R_1 , R_2 , R_3 , L_1 , L_c , and d_c . The stiffness K_s and precompression x_{s0} of returning spring are also need to be optimized to match with solenoid. For simplification, the $K_s = 11$ N/mm is selected, and only the x_{c0} is optimized. Therefore, there are total of seven parameters should be optimized.

B. Optimization Objectives

In the present study, the requirement of HSV include quick response, long time durability, and small size. According to these requirements, we define the optimization objectives include opening time t_{on} , closing time t_{off} , the saturation temperature T_s under rated force, and the length of solenoid L_m . All those objectives will be discussed as follows.

1) Opening time t_{on} .

The schematic diagram of opening and closing processes are shown in Fig. 6. When the valve switches from opening to closing, the two ends of coil are connected to a voltage source. The current will increase and when the magnetic force is bigger than the preload of spring, the plunger starts to open until it reaches the maximum displacement. When the valve switches from closing to opening, the two end of coil are connected to a resistance. The energy stored in the reluctance begins to dissipate. The current decreases and when the magnetic force is smaller than the returning spring force, the plunger starts to close until it reaches the closing position.

The t_{on} is defined as the time during step input voltage and until the valve is fully opened. There are two segments in the opening process. The first segment is the current increases after step input voltage U_s until the output force is bigger than the spring preload. It is a first order system and the current in time domain can be presented as

$$i(t) = \frac{U_s}{R_e} (1 - e^{-\frac{1}{\tau_{eon}} t}) \quad (29)$$

where time constant $\tau_{eon} = L_e/R_e$, and $R_e = \rho_c L_c/s_c$ and $L_{e1} = N^2/(R_{tot1})$ are resistance and inductance of winding, respectively. R_{tot1} is total reluctance when plunger is at opening position.

Equation (28) indicates that the F_m is proportional to the square of B_g while B_g is proportional to input current i . Therefore, the first segment of t_{on} can be calculated by $i(t_{on1}) = i_{cp}$, where i_{cp} is the current to overcome the spring preload. The time t_{on1} can be obtained by (29).

The second segment is during the plunger begins to move at t_{on1} until the plunger reaches the end of stroke, which can be denoted as t_{on2} . This segment is much more complicated than the first segment. Even if neglect the nonlinear of current to force, it should be a third-order system. Since the plunger is limited in a very short stroke, a simplified method which only considers it as a uniformly acceleration process is used in the present study, which is calculated by

$$t_{on2} = \sqrt{2x_s/a_{on}} \quad (30)$$

where $a_{on} = (F_{m0} - K_s x_{c0})/m$, F_{m0} is the magnetic force at initial position, and m is the mass of spool. It is a conservative assumption that suits for preliminary design optimization.

2) Closing time t_{off} .

The t_{off} is defined as the time during cut of voltage and switch to connect resistance until the valve is closed completely. The closing process is also can be divided into two phase. The first stage is current decrease before plunger begin to move. The current in time domain can be presented as

$$i(t) = I_{hold}(t) e^{-\frac{1}{\tau_{eoff}} t} \quad (31)$$

where $\tau_{eoff} = L_{eoff}/R_{eoff}$. In the present study, in order to close the HSV rapidly, a resistance of 1 k Ω is connected between two end of coil to decrease the time constant. The t_{off1} can be calculated by $i(t_{off1}) = i_{cl}$, where i_{cl} is the minimum current to hold the plunger at opening position. Then, t_{off1} can be calculated by (31).

The second phase is the time of begin to move until fully open. Similar to the opening process, since the stroke of spool is limited, the closing time is calculated by an uniformly acceleration process, which is calculated by

$$t_{off2} = \sqrt{2x_s/a_{off}} \quad (32)$$

where $a_{off} = K_s(0.5x_s + x_{c0})/m$.

3) Saturation temperature T_s .

The HSV needs to keep opening for a long time under sustain load, which is mostly decided by the thermal performance. As current flows through the winding, the winding generates heat causing the temperature to rise, and the heat dissipates into the environment through the surface of coil. When the solenoid continuously outputs rated force, the heat generation and dissipation will reach a dynamic equilibrium at a constant temperature, which can be defined as saturation temperature T_s . The sustain load is set as 10 N.

High saturation temperature will increase resistance, reduce the electromagnetic force, and even make the HSV failure. Therefore, it is important to verify that the magnitude of the saturation temperature under rated force is low enough. Calculate the required current for rated output force then using

following equation to get the $T_s = T_{\text{env}} + \Delta T$:

$$a\Delta T^2 + (b - C)\Delta T = C(T_{\text{env}} + 234.5) \quad (33)$$

where C is a constant which can be calculated by $C = I^2 R_{20} / (A_{\text{dis}}(234.5 + 20))$, T_{env} is temperature of environment, $T_s = T_{\text{env}} + \Delta T$, R_{20} is the resistance at 20 °C, a and b are dissipation coefficient, and A_{dis} is dissipation area of coil, which can be calculated by the following equation:

$$A_{\text{dis}} = \frac{\pi(n_c - 1)C_d}{2} \times \{\pi(2R_t + C_d(2m_c - 1)) + \pi(2R_t + C_d)\} + \pi C_d m_c l_{ca} \quad (34)$$

where the number of coil axial layers $n_c = [L_c / C_d]$, the number of radial layers of the coil $m_c = [(R_3 - R_2 - t_1) / C_d]$, the average length of windings $l_{ca} = \pi(R_3 + R_2 + t_1)$, and inner diameter of coil $R_t = R_2 + t_1$.

4) The length of the solenoid L_m .

Small size is also very important for some applications, such as for aerospace. The length of solenoid is mainly decided by L_c , L_1 , and L_2 ; therefore, the length index is defined as $L_m = L_1 + L_2 + L_c$.

The final objective functions are expressed as follows:

$$\text{Objs} = [\text{Obj}_1, \text{Obj}_2, \text{Obj}_3, \text{Obj}_4] = [t_{\text{on}}, t_{\text{off}}, T_s, L_m]. \quad (35)$$

C. MOO Problem Description and Method

This is a MOO problem that needs to find a solution that weighs between objectives and gets the best performance. The advanced way is using a MOO algorithm to obtain the Pareto front and then select the best solution by the MOD method. These design parameters are obtained according to the flow chart shown in Fig. 7. According to MOO and MOD method, a wide design space will be achieved and the optimized design will be selected from the wide design space.

The problem can be defined as: let $S \in R^n$ be an n -dimensional search space, and $f_i(\mathbf{x})$ be k objective functions, $g_j(\mathbf{x})$ be m inequality constraints, defined over S . Let \mathbf{f} be a vector function defined as

$$\mathbf{f}(\mathbf{x}) = [f_1(\mathbf{x}), f_2(\mathbf{x}), \dots, f_k(\mathbf{x})], \quad i = 1, \dots, k$$

where $g_j(\mathbf{x}) \leq 0, \quad j = 1, \dots, m. \quad (36)$

Then, it is interesting to find a solution, $\mathbf{x} = (x_1, \dots, x_n)$, which minimizes $\mathbf{f}(\mathbf{x})$. The objective functions $f_i(\mathbf{x})$ may conflict with each other, thereby, rendering it impossible to detect a single global minimum at the same point in S . Usually, a solution \mathbf{x} , is said to be Pareto optimal, if and only if there is no other solution, \mathbf{y} , in S such that $\mathbf{f}(\mathbf{y})$ dominates $\mathbf{f}(\mathbf{x})$. The set of all Pareto optimal solutions is called the Pareto front.

For MOO method, the multiobjective particle swarm optimization (MOPSO) method [32] is adopted for its good global searching capability and ease of application. The pseudo code of MOPSO in the present study can be described as follows:

- 1) Initialize the population S^{POP} with the random design parameters in the defined range.
- 2) Evaluate each of the particles in S^{POP} , get the performances by EMC model.

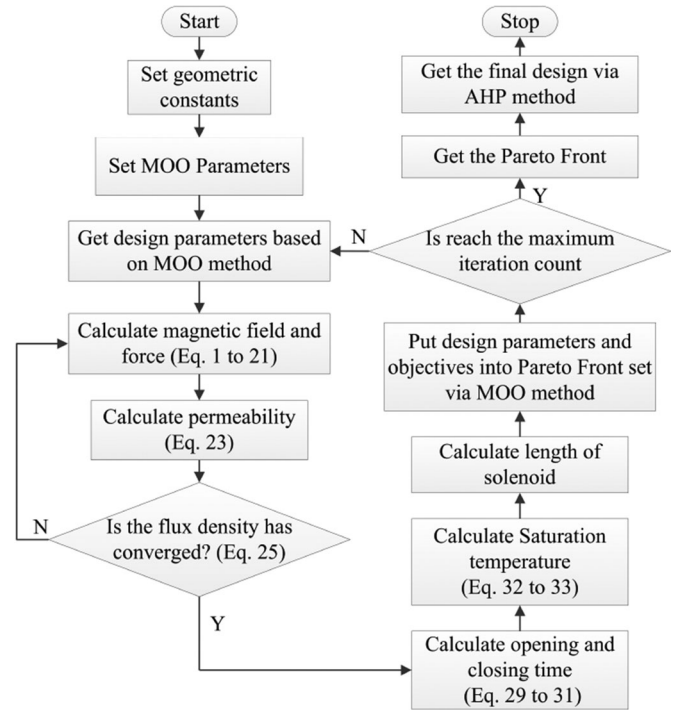


Fig. 7. Design flowchart in present study.

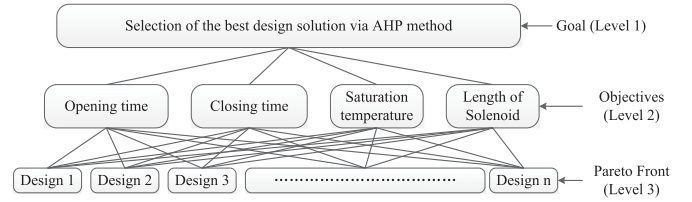


Fig. 8. Analytic Hierarchy Process diagram.

- 3) Store the positions (design parameters) that get the non-dominant performances into the repository S^{REP} .
- 4) Restore the repository to make it well-distributed, keep the size of repository under the defined capacity.
- 5) Compute the update speed of each particle using

$$v_i(t+1) = wv_i(t) + c_1r_1(p_i^{\text{BEST}}(t) - x_i(t)) + c_2r_2(R_h(t) - x_i(t)) \quad (37)$$

where p_i^{BEST} is its best position in searching history, R_h is the selected leader from the repository, w is the inertia coefficient of velocity, c_1 and c_2 are local and social coefficients, respectively, and r_1 and r_2 are two random numbers in range $[0,1]$.

- 6) Compute the new position of the particles by adding the speed produced from the previous step, $S_i^{\text{POP}}(t+1) = S_i^{\text{POP}}(t) + v_i(t)$, and get new positions and return back to the Step 2 until maximum iteration cycle is reached.

For MOD method, the analytic hierarchy process principle (AHP) method can break down complex problems into parts and then puts them into a hierarchical framework. At the top level of hierarchy lies decision objective, the lower levels of the hierarchy contain criteria, and the last level contains the decision

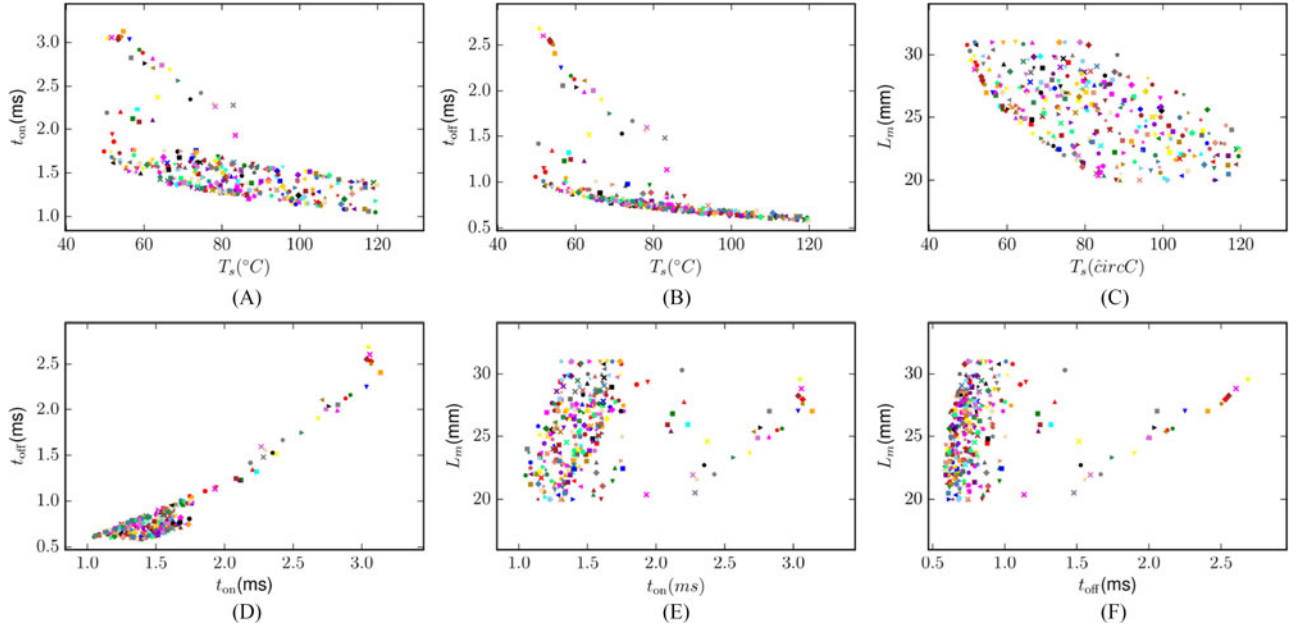


Fig. 9. Optimization results of pareto front of each two objectives. (A) T_s versus T_{on} . (B) T_s versus T_{off} . (C) T_s versus L_m . (D) T_{on} versus T_{off} . (E) T_{on} versus L_m . (F) T_{off} versus L_m .

alternatives. The priority of the problem parts is defined by pairwise comparisons. It is easier and more accurate to express one's opinion on only two elements than simultaneously on all of the elements. The decision maker does not need to provide a numerical judgment, nevertheless, a relative verbal appreciation is more familiar in our daily lives. The AHP method has been applied in a limited angle motor design in [20], and the details can be referred.

A three-level hierarchy framework for solenoid is shown in Fig. 8. Level one presents the overall goal of decision making which is selection of the best design based on the application requirements. The second level is the objectives previously mentioned. The third level identifies the design solutions in the Pareto front, which is obtained by MOO method.

D. Optimization Results

In order to facilitate the range setting, replace R_3 , R_2 , R_1 using t_s , t_c , t_m . The parameters range are listed below: $t_s \in [1.2, 2]$, $t_c \in [1.7, 3]$ mm, $t_m \in [2, 3.5]$ mm, $L_1 \in [2, 4]$ mm, $L_c \in [10, 25]$ mm, $d_c \in [0.2, 0.6]$ mm, and $x_{c0} = [0.2, 0.6]$ mm. Maximum optimization iteration of MOPSO is 100, the particle count is set as 600 and the capacity of the repository are set as 300. The obtained pareto front that includes 300 solutions is shown in Fig. 9.

The subfigures in Fig. 9 are 2-D scatter plots of each two objectives. Fig. 9(A) and (B) indicate that both t_{on} and t_{off} are conflicting with T_s that means improving durability of temperature, such as improving cooling condition, is benefit for improving dynamic performance. Fig. 9(C) indicates that the L_m is also conflict with T_s . Fig. 9(D) indicates t_{on} and t_{off} are in a positive relationship which means they can improve in the same time. Fig. 9(E) and (F) present that the L_m is positive correlation with t_{on} and t_{off} , and the possible reason could

TABLE II
TWO DIFFERENT COMPARISONS MATRIX OF EACH OBJECTIVES OF AHP

Cases	Objectives	T_s	t_{on}	t_{off}	L_m	Weight
Case 1	T_s	1	5/5	5/3	5/1	0.357
	t_{on}	5/5	1	5/3	5/1	0.357
	t_{off}	3/5	3/5	1	3/1	0.214
	L_m	5/1	5/1	1/3	1	0.071
Case 2	T_s	1	3/5	3/7	3/1	0.1875
	t_{on}	5/3	1	5/7	5/1	0.3125
	t_{off}	7/3	7/5	1	7/1	0.4375
	L_m	1/3	1/5	1/7	1	0.0625

be that the shorter mover has smaller mass. Each point with the same color and same marker indicates the same solution.

There are 300 valid solutions in pareto front after MOO process. It is still hard for designer to decide which solution should be selected and some method should be applied to compare these solution. The best solution is selected via AHP method in the present study. Different priority vector of objectives will result in different best solutions. Two cases of priority vectors are presented in Table II. The case 1 regard saturation temperature is the same important as opening and closing time, and case 2 regard saturation temperature is less important than opening and closing time. Fig. 10 shows the normalized value of AHP over all weight percentages of all solutions in the pareto front of these two cases. Best solution and objectives of each case are highlighted in the figure. The radargraph of these two cases are shown in Fig. 11. It indicate the different of these two solutions clearly.

Taking the manufacturing considerations and the AHP results into account, the final rounded parameters of the selected

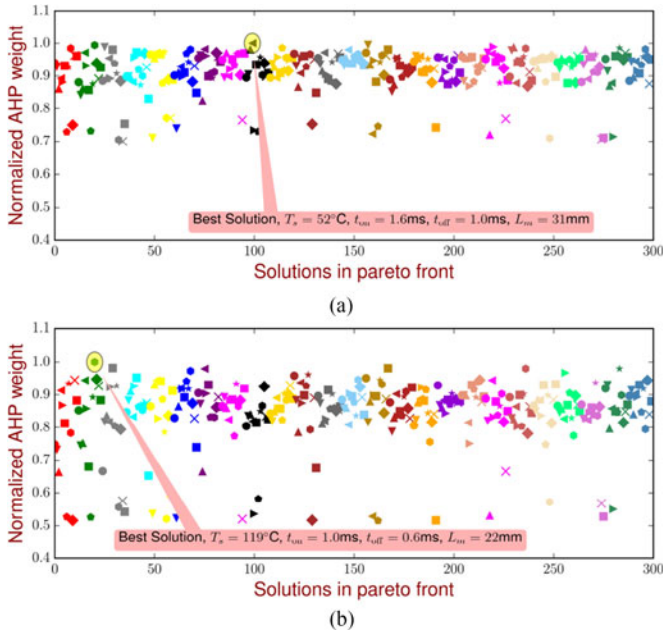


Fig. 10. AHP overall weight percent for solutions in pareto front. (a) Case 1. (b) Case 2.

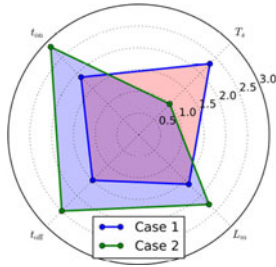


Fig. 11. Radar graphic of case 1 and 2.

solution are $t_s = 1.7$, $t_c = 2.8$ mm, $t_m = 2.4$ mm, $L_1 = 2.5$ mm, $L_c = 18$ mm, $d_c = 0.25$ mm, and $x_{c0} = 0.45$ mm.

V. PROTOTYPE AND EXPERIMENTS

Based on the final optimization results, several prototypes were manufactured. The resistance and inductance of solenoid are $15\ \Omega$ and $40\ \text{mH}$, respectively. The static force performance is tested with the input current density of $6\ \text{A/mm}^2$ and the output force and the displacement of the plunger are measured. The curve of force versus displacement is shown in Fig. 12. It can be seen that the experimental results are consistent with the simulation results well. The minimum force at the initial position is bigger than $10\ \text{N}$, which meets the requirements.

The displacement of the plunger cannot be obtained directly since the plunger is completely wrapped by the shell. Therefore, a test rig which uses two HSVs and a pressure transducer to check the dynamic performance is set up and shown in Fig. 13. The HSV connecting to the low pressure tank keeps open as an orifice. Another HSV which is connected to a high pressure source ($9\ \text{MPa}$) is closed at the initial state. The pressure transducer will detect the incre-

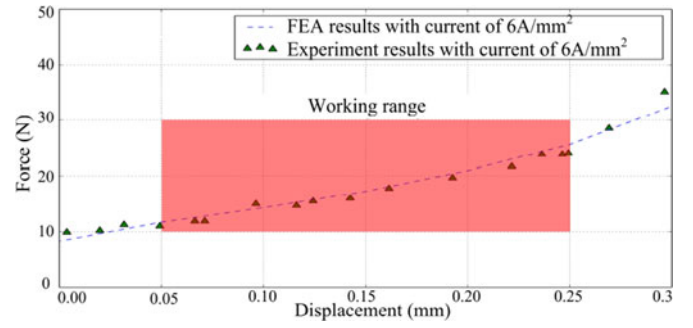


Fig. 12. Static force versus displacement.

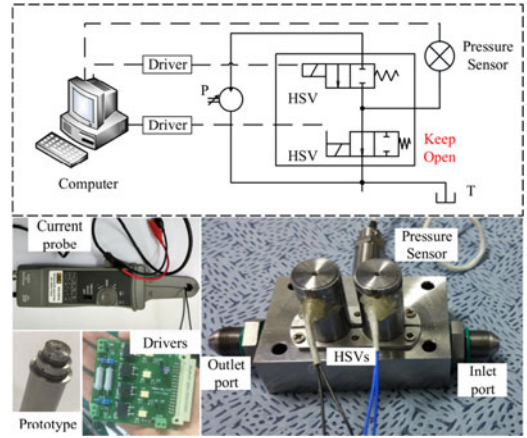


Fig. 13. Experimental setup for dynamic performance.

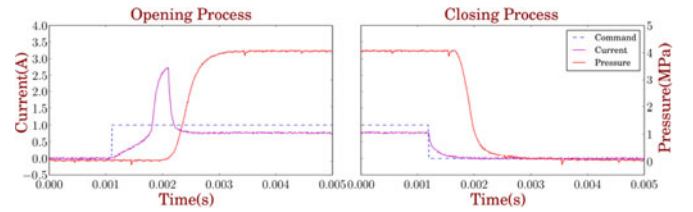


Fig. 14. Experiment result of dynamic performance.

ment of the pressure, which is proportional to the opening displacement of HSV. A current probe (ETA5301A) is used to detect the dynamic of the winding current. A driver is developed to control the on/off valve which can connect a high voltage source in the beginning to achieve high speed open and switch to a low voltage source after the valve opened to reduce heat and save energy.

The drive gives a $24\ \text{V}$ step voltage to open the HSV and changes to $12\ \text{V}$ after $1\ \text{ms}$. The dynamic of opening and closing process are shown in Fig. 14. The results indicate that the current is arising after the input voltage. When the current is over $0.6\ \text{A}$, the plunger begins to open the seal ball and the pressure begins to increase. The pressure curve indicates that the valve is fully opened in $2.4\ \text{ms}$. The current and pressure curves of closing process indicate that the valve is fully closed in $2\ \text{ms}$. The opening and closing time are both a little longer than the optimization results and could be due to the winding turns being less than the ideal value.

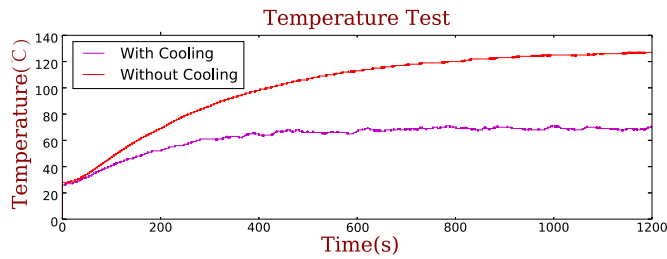


Fig. 15. Experimental results of saturation temperature.

The saturation temperature with rated current is tested, which is shown in Fig. 15. The saturation temperature is lower than 130 °C without cooling, and it is lower than 60 °C with fan cooling. It is below the critical value of the winding that even agrees with the optimization results.

VI. CONCLUSION

This paper presented the design and the optimization of a hollow plunger type solenoid for HSV. The proposed solenoid has oil through hole in the middle of the plunger to connect the two ends of the plunger, which allows the oil in the two end chambers to pass through when the plunger is moving. This design decreases the circular air gap, enhances the magnetic force, and reduces the mass of the mover. An accurate equivalent magnetic circuit model is developed for solenoid optimization. The magnetic circuit is arranged in Kirchhoff voltage law matrix form for computer calculation convenience. An iterative method is utilized for obtain accurate permeability of the nonlinear magnetic material. The theoretical model of opening and closing time and saturation temperature are delivered for optimization. The multiobjective particle swarm optimization method is utilized to obtain the Pareto front of desired objectives. The optimum solution in Pareto front is selected by the analytic hierarchy process, and prototypes are carried out based on the optimization results. The test results of static force characteristics and dynamic response are proven to be consistent with the optimization results, which indicates the feasible of the proposed optimization method.

REFERENCES

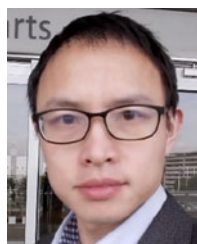
- [1] M. Linjama, A. Laamanen, and M. Vilenius, "Is it time for digital hydraulic?" in *Proc. 8th Scand. Int. Conf. Fluid Power*, Tampere, Finland, May 2003.
- [2] F. Wang, L. Gu, and Y. Chen, "A hydraulic pressure-boost system based on high-speed on/off valves," *IEEE/ASME Trans. Mechatron.*, vol. 18, no. 2, pp. 733–743, Apr. 2013.
- [3] Y. C. Feng Wang and L. Gu, "A continuously variable hydraulic pressure converter based on high-speed on/off valves," *Mechatron.*, vol. 21, no. 8, pp. 1298–1308, 2011.
- [4] Y. Zeng, D. Wang, B. Zi, and Q. Zeng, "Dynamic characteristics of priority control system for high-speed on/off digital valve," *Adv. Mech. Eng.*, vol. 7, no. 4, pp. 1–8, 2015.
- [5] Z. Kangwu, G. Linyi, C. Yuanjie, and L. Wei, "High speed on-off valve control hydraulic propeller," *Chin. J. Mech. Eng.*, vol. 25, no. 3, pp. 463–473, 2012.
- [6] Y. Shi, C. Liu, and Y. Zhang, "Design and study of a new kind of larger flow rate high-speed on-off valve," *Chin. J. Mech. Eng.*, vol. 40, no. 4, pp. 195–198, 2005.
- [7] L. Li, C. Zhang, B. Yan, and X. Li, "Research of a giant magnetostrictive valve with internal cooling structure," *IEEE Trans. Magn.*, vol. 47, no. 10, pp. 2897–2900, Oct. 2011.
- [8] G. Xue, P. Zhang, Z. He, D. Li, Y. Huang, and W. Xie, "Design and experimental study of a novel giant magnetostrictive actuator," *J. Magn. Mater.*, vol. 420, pp. 185–191, 2016.
- [9] D. L. Proctor, D. R. Albert, and H. F. Davis, "Improved piezoelectric actuators for use in high-speed pulsed valves," *Rev. Sci. Instrum.*, vol. 81, no. 2, Feb. 2010, Art. no. 023106.
- [10] H. Mutai and K. Yamasawa, "Fundamental operations of a multipolar disk-solenoid," *IEEE Trans. Magn.*, vol. 31, no. 4, pp. 2445–2449, Jul. 1995.
- [11] A. B. J. Sung and B. D. S. Kim, "A design method of voice coil type high speed actuator for valve operation," in *Proc. 15th Int. Conf. Electr. Mach. Syst.*, 2012, pp. 1–5.
- [12] X. Kong and S. Li, "Dynamic performance of high speed solenoid valve with parallel coils," *Chin. J. Mech. Eng.*, vol. 27, no. 4, pp. 816–821, 2014.
- [13] B. Han, Q. Xu, and Q. Yuan, "Multiobjective optimization of a combined radial-axial magnetic bearing for magnetically suspended compressor," *IEEE Trans. Ind. Electron.*, vol. 63, no. 4, pp. 2284–2293, Apr. 2016.
- [14] S. Li, P. Guo, W. Jiang, H. Ding, and D. Yu, "Research on response characteristics and parameters optimization of high-speed solenoid valve," in *Proc. 34th Chin. Control Conf.*, 2015, pp. 2327–2332.
- [15] A.-C. Zavoianu, G. Bramerdorfer, E. Lughofer, S. Silber, W. Amrhein, and E. P. Klement, "Hybridization of multi-objective evolutionary algorithms and artificial neural networks for optimizing the performance of electrical drives," *Eng. Appl. Artif. Intell.*, vol. 26, no. 8, pp. 1781–1794, Sep. 2013.
- [16] D. K. Lim, K. P. Yi, S. Y. Jung, H. K. Jung, and J. S. Ro, "Optimal design of an interior permanent magnet synchronous motor by using a new surrogate-assisted multi-objective optimization," *IEEE Trans. Magn.*, vol. 51, no. 11, Nov. 2015, Art. no. 8207504.
- [17] F. Cupertino, G. Pellegrino, and C. Gerada, "Design of synchronous reluctance motors with multiobjective optimization algorithms," *IEEE Trans. Ind. Appl.*, vol. 50, no. 6, pp. 3617–3627, Nov. 2014.
- [18] H. Duan and L. Gan, "Orthogonal multiobjective chemical reaction optimization approach for the brushless DC motor design," *IEEE Trans. Magn.*, vol. 51, no. 1, pp. 1–7, Jan. 2015, Art. no. 7000207.
- [19] K. Yamazaki and H. Ishigami, "Rotor-shape optimization of interior-permanent-magnet motors to reduce harmonic iron losses," *IEEE Trans. Ind. Electron.*, vol. 57, no. 1, pp. 61–69, Jan. 2010.
- [20] R. Nasiri-Zarandi, M. Mirsalim, and A. Cavagnino, "Analysis, optimization, and prototyping of a brushless DC limited-angle torque-motor with segmented rotor pole tip structure," *IEEE Trans. Ind. Electron.*, vol. 62, no. 8, pp. 4985–4993, Aug. 2015.
- [21] S. Wu, X. Zhao, X. Li, P. C. K. Luk, and Z. Jiao, "Preliminary design and optimization of toroidally wound limited angle servo motor based on a generalized magnetic circuit model," *IEEE Trans. Magn.*, vol. 52, no. 9, pp. 1–9, Sep. 2016.
- [22] Y. S. Chen, Z. Q. Zhu, and D. Howe, "Slotless brushless permanent magnet machines: Influence of design parameters," *IEEE Trans. Energy Convers.*, vol. 14, no. 3, pp. 686–691, Sep. 1999.
- [23] H. I. Lee and M. D. Noh, "Design and control of radial-flux toroidally wound brushless DC machines," *IEEE Trans. Ind. Electron.*, vol. 58, no. 2, pp. 444–449, Feb. 2011.
- [24] K. Chau, M. Cheng, and C. Chan, "Nonlinear magnetic circuit analysis for a novel stator doubly fed doubly salient machine," *IEEE Trans. Magn.*, vol. 38, no. 5, pp. 2382–2384, Sep. 2002.
- [25] H. Polinder, J. G. Sloopweg, M. J. Hoeijmakers, and J. C. Compter, "Modeling of a linear PM machine including magnetic saturation and end effects: Maximum force-to-current ratio," *IEEE Trans. Ind. Appl.*, vol. 39, no. 6, pp. 1681–1688, 2003.
- [26] Y. Liu, M. Zhang, Y. Zhu, J. Yang, and B. Chen, "Optimization of voice coil motor to enhance dynamic response based on an improved magnetic equivalent circuit model," *IEEE Trans. Magn.*, vol. 47, no. 9, pp. 2247–2251, Nov./Dec. 2011.
- [27] C. Pompermaier, K. Kalluf, A. Zambonetti, M. Luz, and I. Boldea, "Small linear PM oscillatory motor: Magnetic circuit modeling corrected by axisymmetric 2-D FEM and experimental characterization," *IEEE Trans. Ind. Electron.*, vol. 59, no. 3, pp. 1389–1396, Mar. 2012.
- [28] J. R. Brauer, *Magnetic Actuators and Sensors*. New York, NY, USA: Wiley, 2006.
- [29] S. Wu, X. Zhao, Z. Jiao, P. C. K. Luk, and C. Jiu, "Multi-objective optimal design of a toroidally wound radial-flux halfbach permanent magnet array limited angle torque motor," *IEEE Trans. Ind. Electron.*, vol. 64, no. 4, pp. 2962–2971, Apr. 2016.

- [30] J. A. Tapia, J. Pyrhonen, J. Puranen, P. Lindh, and S. Nyman, "Optimal design of large permanent magnet synchronous generators," *IEEE Trans. Magn.*, vol. 49, no. 1, 3, pp. 642–650, Jan. 2013.
- [31] H. C. Roters, *Electromagnetic Devices*. London Chapman & Hall: New York, NY, USA: Wiley, 1941.
- [32] C. Coello, G. Pulido, and M. Lechuga, "Handling multiple objectives with particle swarm optimization," *IEEE Trans. Evol. Comput.*, vol. 8, no. 3, pp. 256–279, Jun. 2004.



Chunfang Li was born in ShanXi, China, in 1993. She received the Bachelor's degree in electrical engineering from the Department of Mechanical Engineering, North China Electric Power University (Baoding), Beijing, China, in 2016. She is currently working toward the Master's degree in mechatronic engineering the School of Automation Science and Electrical Engineering, Beihang University, Beijing.

Her research interests include mechatronics, modeling, and simulation.



Shuai Wu (M'15) received the Ph.D. degree in mechatronics engineering from Beihang University, Beijing, China, in 2011.

From 2011 to 2013, he was a Postdoctoral Fellow at Beihang University, where he has been a Lecturer since 2013. His research interests include hydraulic servo control of aircraft, modeling and simulation, dynamics and control of mechatronic systems, and advanced electrical and hydraulic servo components.



Zongxiao Jiao (M'11–SM'13) received the B.S. degree in fluid power and transmission and Ph.D. degree in mechatronic engineering from Zhejiang University, Hangzhou, China, in 1985 and 1991, respectively.

From 1991 to 1993, he was a Postdoctoral Fellow at Beihang University, Beijing, China, where he has been a Professor since 1994. He is currently the Dean of the School of Automation Science and Electrical Engineering at Beihang University. His research interests include actuators, sensors, fluid power, and more electrical aircraft.

Dr. Jiao received the Changjiang Scholar Professor in 2006 and the Distinguished Young Scholar of China in 2008.



Xiangyu Zhao was born in Hebei, China, in 1993. He received the B.S. degree in automation from the Automation School of Beiyu University Beijing, Beijing, China, in 2015. He is currently working toward the M.S. degree in mechatronic engineering in the School of Automation Science and Electrical Engineering, Beihang University, Beijing.

His research interests include mechatronics, advanced electrical-hydraulic servo components, modeling, and simulation.



Yufeng Qu received the B.S. degree in mechanical design and M.S. degree in mechanical design and theory from the School of Mechanical Engineering, Hefei University of Technology, Hefei, China, in 2004 and 2008, respectively. He received the Ph.D. degree in mechatronic engineering from Robotics Institute, School of Mechanical Engineering and Automation, Beihang University, Beijing, China, in 2014.

He is currently a Postdoctoral Fellow in the School of Automation Science and Electrical Engineering, Beihang University. His research interests include robotics, parallel mechanisms, and mechanical and electrical engineering.